Accepted Manuscript

Published online: 26 Sept. 2026

Doi: 10.34172/japid.5482

Submitted: August 06, 2026

Revised: September 07, 2026

Accepted: September 09, 2026

Original article

CBCT metal artifact profiles of different dental implant brands: An in vitro evaluation of metal artifact reduction

Sema Kaya[1*] • Onur Sahar[2]

[1]Department of Oral and Maxillofacial Radiology, Faculty of Dentistry, Van Yuzuncu Yil University, Van, Turkey
[2]Department of Oral and Maxillofacial Surgery, Faculty of Dentistry, Van Yuzuncu Yil University, Van, Turkey
ORCID: Sema Kaya: 0000-0002-6306-3901
ORCID and Email: Onur Sahar: onursahar@gmail.com, 0009-0000-5105-5093

[*]**Corresponding Author; Email:** semakaya@yyu.edu.tr

Abstract

Background. Metal artifacts from dental implants may compromise cone-beam computed tomography (CBCT) image quality and complicate radiographic assessment of peri-implant structures. Although metal artifact reduction (MAR) algorithms are widely available, their effectiveness may vary according to implant characteristics. This study aimed to evaluate CBCT gray-value artifact profiles of different commercially available dental implant brands and to assess the effect of MAR under standardized in vitro conditions.

Methods. Eleven commercially available dental implant systems were individually embedded in a standardized wax phantom and scanned using a CS 9600 CBCT unit with identical acquisition parameters (120 kVp, 5 mA, 12 s, 12×5-cm field of view, and 0.3-mm voxel size). Each implant was scanned three times and reconstructed with and without MAR. Gray-value measurements were obtained from eight standardized circular regions of interest positioned around each implant at the coronal, middle, and apical axial levels, and corresponding measurements from the three levels were averaged. The overall effect of MAR was evaluated using paired brand-level mean values, while exploratory implant-specific comparisons were adjusted using the Holm method.

Results. A total of 528 region-of-interest measurements were analyzed. Under standardized, uniform wax-phantom conditions, the overall mean gray-value artifact measurement decreased from 41.08 without MAR to 37.89 with MAR, a reduction of 3.19 gray-value units (7.8%); however, this difference was not significant (Wilcoxon signed-rank test, P=0.206). Artifact values decreased in eight of the 11 evaluated implant specimens and increased in three. After Holm adjustment for multiple comparisons, significant differences remained for iRES (adjusted P=0.001), Medigma (adjusted P=0.031), Straumann (adjusted P<0.001), and NTA (adjusted P=0.005). MAR was associated with lower artifact values for iRES and Straumann but higher values for Medigma and NTA.

Conclusion. The evaluated implant specimens exhibited different CBCT gray-value artifact profiles and heterogeneous responses to MAR activation under standardized experimental conditions. MAR produced a numerical reduction in the overall mean artifact measurement, but the overall change was not significant. Moreover, its effect was not uniformly reductive across the evaluated specimens. Because only one implant represented each brand, these findings should be interpreted as specimen-level descriptive observations rather than generalized evidence of brand-specific radiographic behavior. The observed quantitative gray-value changes should not be interpreted as direct evidence of improved diagnostic performance in

assessing peri-implant bone defects. These in vitro findings were obtained in a uniform wax phantom and cannot be directly extrapolated to clinical peri-implant bone assessment or diagnostic performance.

Graphical abstract

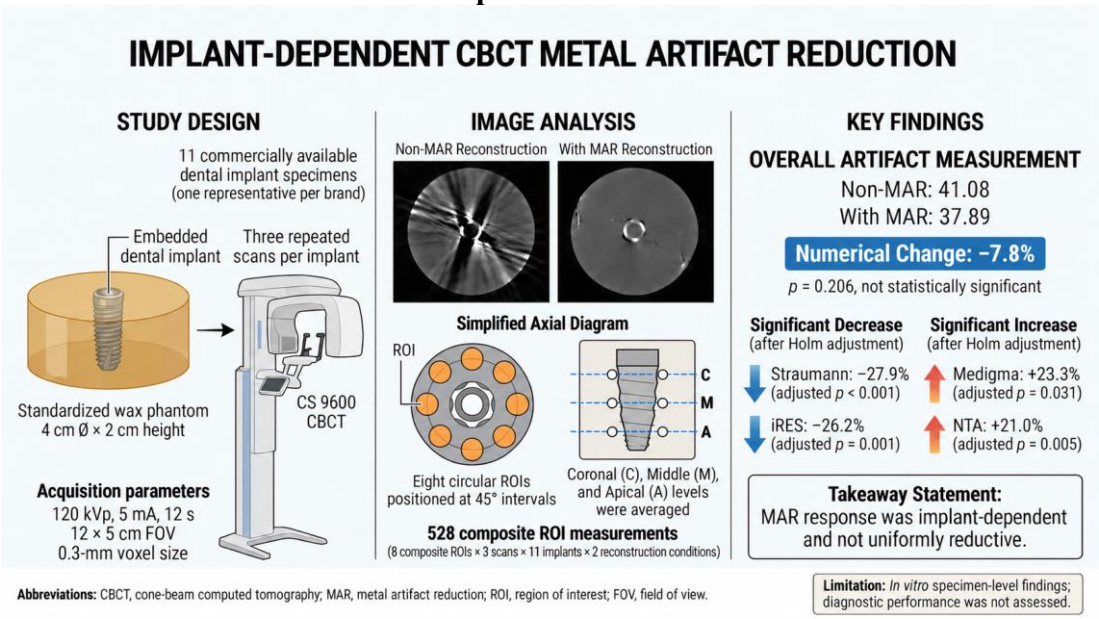

Key words: Cone-beam computed tomography, dental implants, image quality, metal artifact reduction, peri-implant bone assessment, presurgical planning.

Introduction

Dental implants are a well-established treatment modality for rehabilitating partially and completely edentulous patients. Advances in implant surface technology, macrodesign, surgical protocols, and prosthetic planning have improved the predictability of implant therapy and expanded its clinical indications.[1] However, the increasing number of implant-supported restorations has also increased the need for accurate postoperative assessment of peri-implant tissues. Peri-implantitis is characterized by inflammation of peri-implant soft tissues together with progressive loss of supporting bone, and radiographic evaluation of peri-implant bone loss remains an essential component of diagnosis and follow-up.[2,3]

Intraoral radiography is commonly used for routine postoperative implant monitoring because it is accessible, inexpensive, and associated with relatively low radiation exposure. Nevertheless, conventional two-dimensional radiographs have inherent limitations, particularly for evaluating buccal and lingual bone surfaces, circumferential defects, fenestrations, dehiscences, and the spatial relationship between implants and adjacent anatomical structures. Cone-beam computed tomography (CBCT) provides multiplanar and three-dimensional evaluation of the maxillofacial skeleton and has therefore become an important adjunctive imaging modality in implant dentistry when conventional radiography and clinical findings are insufficient.[4,5] Previous experimental and systematic studies have shown that CBCT may be useful for the assessment of peri-implant bone defects, especially buccal marginal defects, fenestrations, and dehiscences.[6,7]

Despite these advantages, metallic objects can substantially compromise CBCT image quality. Dental implants may generate artifacts through beam hardening, photon starvation, scatter radiation, extinction effects, and partial-volume averaging.[8,9] These artifacts may appear as streaks, dark bands, cupping effects, and irregular gray-value changes around the implant body. This image degradation may obscure the bone–implant interface and reduce the reliability of

peri-implant bone assessment, particularly in regions where early peri-implant bone loss or cortical defects should be detected.[8–10]

The severity of implant-related artifacts is influenced by several imaging and object-related factors. CBCT device type, field of view, voxel size, tube voltage, exposure protocol, reconstruction algorithm, anatomical region, bone density, and the position of metallic objects within the scanned volume may all affect artifact expression. Implant-related factors may also contribute to this variability. Studies comparing different implant materials have shown that titanium, titanium-zirconium, and zirconium dioxide implants may produce different artifact patterns and gray value alterations in CBCT images.[9,11–13] These findings indicate that dental implants should not be treated as radiographically identical objects, even when evaluated under similar imaging conditions.

Metal artifact reduction (MAR) algorithms have been incorporated into CBCT systems to reduce artifact expression around high-density materials and improve image interpretability. However, the clinical and quantitative benefits of MAR remain inconsistent. Parsa et al.[14] reported that MAR did not fully correct gray value alterations around titanium implants, suggesting that its effect may depend on the CBCT system and reconstruction protocol.[14] Similarly, de-Azevedo-Vaz et al.[15] found that MAR did not necessarily improve the detection of peri-implant fenestrations and dehiscences under all scanning conditions.[15] Therefore, MAR should not be assumed to provide a uniform improvement in every implant-related CBCT examination.

Although several studies have investigated implant-related CBCT artifacts, most have focused on a limited number of implant materials, selected exposure parameters, specific CBCT devices, or particular phantom configurations.[10–14,16] Comparative evidence regarding artifact formation among different commercially available dental implant brands remains limited. This issue is clinically relevant because implant systems may differ in alloy composition, surface characteristics, thread geometry, macrodesign, and implant–abutment connection design, all of which may theoretically influence x-ray attenuation and artifact expression around the implant body.[17,18] Moreover, when multiple implants or metallic objects are scanned within the same phantom or in adjacent regions, the quantity and position of metal structures may increase artifact expression and complicate the independent assessment of each implant.[16] Evaluating each implant separately under standardized imaging conditions may therefore provide clearer information about the specimen-specific artifact behavior of implants from different brands.

Therefore, this in vitro study aimed to describe the CBCT gray value artifact profiles of different commercially available dental implant brands and to evaluate the effect of a MAR algorithm under standardized acquisition and reconstruction conditions. Brand-related artifact profiles were evaluated descriptively because one representative implant was assessed for each brand. The statistical null hypothesis was that MAR activation would not significantly change overall gray value artifact measurements compared with non-MAR reconstructions.

Methods

Study Design

An in vitro material design was used to evaluate gray value alterations produced by different dental implant brands and to assess the effect of the MAR algorithm. Since the study did not involve human participants, human-derived tissues, animals, patient records, or identifiable patient data, ethics committee approval was not required.

Implant Materials and Preparation

The study included eleven commercially available dental implant systems with comparable macrogeometry and dimensions. Implant diameters ranged from 3.75 to 4.1 mm, and implant

lengths ranged from 10 to 11.5 mm. The manufacturer and country of origin of each implant system were recorded according to product labels and publicly available manufacturer information. The evaluated implant systems were as follows: Bilim/Bilimplant (Proimtech Sağlık Ürünleri A.Ş., Istanbul, Türkiye), DTI (DTİ İmplant Sistemleri San. Tic. A.Ş., Gebze/Kocaeli, Türkiye), iRES (iRES SAGL, Mendrisio, Switzerland), Medentika (MEDENTiKA GmbH, Hügelsheim/Calw, Germany), Medigma (Medigma Biomedical GmbH, Wehingen, Germany), Meisinger (Hager & Meisinger GmbH/Meisinger Implants, Neuss, Germany), Mode (Mode Medikal/Mode Implant, Istanbul, Türkiye), Straumann (Institut Straumann AG, Basel, Switzerland), Venus/Venuscon (Medisolaris Sağlık Hizmetleri San. ve Tic. Ltd. Şti., İzmir, Türkiye), Neodent (JJGC Indústria e Comércio de Materiais Dentários S.A./Neodent, Curitiba, Brazil; Straumann Group), and NTA (NTA Implant/Pilatus Swiss Dental GmbH, Switzerland).

A cylindrical baseplate wax block with a diameter of 4 cm and a height of 2 cm was used as a standardized low-density experimental phantom. The phantom was intentionally selected to provide a uniform background and to isolate implant-associated gray value alterations from variability introduced by cortical thickness, trabecular architecture, soft tissues, anatomical structures, and adjacent metallic objects. Each implant was embedded individually in the center of the same wax block and scanned separately under identical acquisition conditions. This approach minimized overlapping and adjacency-related artifacts and enabled controlled specimen-level comparison of the artifact profiles produced by the evaluated implants. The phantom was not intended to reproduce clinical peri-implant tissues or to assess diagnostic performance under in vivo conditions.

Imaging Protocol

All CBCT images were acquired using the CS 9600 system (Carestream Dental, Atlanta, GA, USA). To ensure standardization, the scanning parameters were set as follows: tube voltage: 120 kVp, tube current: 5 mA, exposure time: 12 seconds, field of view (FOV): 12 × 5 cm, voxel size: 0.3 mm, device anatomical preset: mandible.

A 120-kVp protocol was selected to reduce beam-hardening effects and improve acquisition stability under the tested experimental conditions. To reduce acquisition-related variability, each implant was scanned three times using the same parameters. Thus, three repeated acquisitions were obtained for each implant.

Image Reconstruction

The acquired raw data were reconstructed in two different ways:

1. Non-MAR: without using the metal artifact reduction algorithm
2. With MAR: with the device's metal artifact reduction algorithm activated

Image Analysis

Image analyses were performed using ImageJ software (NIH, Bethesda, MD, USA). For each implant, three standardized axial levels corresponding to the coronal, middle, and apical thirds of the implant body were selected. Gray value measurements were obtained from eight standardized circular regions of interest (ROIs), each with a diameter of 3.0 mm (10 pixels) and an ImageJ-measured area of 7.20 mm^2, placed around the implant at 45° intervals at each axial level using the "Analyze → Measure" command (Figure 1). The ROIs were positioned immediately adjacent to the implant surface without overlapping the implant body, and the same ROI size was used for all measurements. The values obtained from the corresponding ROI positions at the three axial levels were averaged to generate eight composite ROI measurements for each scan. Gray value measurements were interpreted as relative markers of peri-implant

gray value alteration within the same CBCT unit, acquisition protocol, and reconstruction condition, rather than as absolute density values.
This procedure was repeated for three separate scans per implant. For each scan, the measurements obtained from corresponding ROI positions at the coronal, middle, and apical axial levels were averaged, yielding eight composite ROI measurements per implant. Because each implant was scanned three times, 24 composite ROI measurements were obtained for each implant under each reconstruction condition. Accordingly, 264 composite ROI measurements were analyzed in the non-MAR condition and 264 in the with-MAR condition, yielding a total of 528 measurements. A radiologist with 13 years of experience in oral, dental, and maxillofacial radiology performed all measurements. To assess intra-observer reliability, the same observer repeated a subset of measurements after a two-week interval, and the intraclass correlation coefficient was calculated. The ICC value was 0.89, indicating good intra-observer reliability.

Statistical Analysis

Statistical analyses were performed using SPSS 25.0 (IBM Corp., Armonk, NY, USA). Descriptive statistics were calculated as mean and standard deviation for each implant brand under non-MAR and MAR reconstruction conditions. Three acquisitions and multiple ROI measurements were used to assess reconstruction-related gray value variations for each tested specimen and did not increase the number of independent implant specimens. Therefore, the effective hardware sample size remained one implant per brand, and no inferential comparisons between implant brands or generalized conclusions regarding overall brand performance were made. For all primary outcomes, two-sided 95% confidence intervals were calculated for the mean values under the non-MAR and MAR conditions and for the paired mean differences between these conditions.
The primary statistical analysis evaluated the overall effect of MAR activation using paired brand-level mean values. This approach was selected to avoid treating repeated ROI-level measurements from the same implant as independent implant specimens. The Wilcoxon signed-rank test was used to compare paired brand-level mean values between non-MAR and MAR reconstructions. For the primary Wilcoxon signed-rank analysis, the Hodges–Lehmann estimator and its 95% confidence interval were calculated to quantify the overall paired difference between the non-MAR and MAR conditions.
In addition, exploratory ROI-level paired comparisons were performed separately for each implant brand using the Wilcoxon signed-rank test. These comparisons were based on paired measurements obtained from corresponding ROI positions and repeated scans under non-MAR and MAR conditions. The eight standardized ROI positions were not analyzed as eight separate hypotheses; instead, they constituted paired observations describing the circumferential artifact profile of each implant. Nevertheless, because separate exploratory comparisons were performed for 11 implant brands, the resulting P-values were adjusted using the Holm method to control the family-wise Type I error rate. Both unadjusted and Holm-adjusted P-values were reported, and statistical significance for these exploratory analyses was evaluated using the adjusted P-values.
The percentage change after MAR activation was calculated using the following formula: [(non-MAR mean – MAR mean)/Non-MAR mean] × 100. Positive values indicated a reduction in gray value artifact measurements after MAR activation, whereas negative values indicated an increase. Because only one representative implant was evaluated for each brand, comparisons between implant brands were interpreted descriptively. The significance level for the primary analysis was set at $P<0.05$.

Results

Table 1 presents the corresponding 95% confidence intervals for the non-MAR and MAR means and the paired mean differences. For each reconstruction condition, 264 composite ROI measurements were obtained from 11 implant specimens, yielding a total of 528 measurements. In the non-MAR condition, the Medigma implant had the lowest mean artifact value (34.03±8.37), followed by the DTI implant (34.14±5.65) and the NTA implant (37.42±9.44). The Straumann implant had the highest mean artifact value (47.18±15.14), followed by the iRES implant (45.65±8.46) and the Mode implant (45.27±13.23) (Table 1). In the MAR condition, the DTI implant had the lowest mean artifact value (32.92±8.77), followed by the iRES implant (33.71±8.12), the Straumann implant (34.03±8.37), and the Bilim implant (35.07±10.14). The highest mean artifact value was observed for the NTA implant (45.27±13.23), followed by the Medigma implant (41.96±11.58) and the Meisinger implant (41.37±14.24) (Table 1).

Before adjustment for multiple comparisons, exploratory ROI-level Wilcoxon signed-rank tests showed significant non-MAR–MAR differences for the Bilim (unadjusted P=0.011), iRES (unadjusted P<0.001), Medentika (unadjusted P=0.009), Medigma (unadjusted P=0.004), Straumann (unadjusted P<0.001), and NTA (unadjusted P<0.001) implants. After Holm adjustment for the 11 implant-specific comparisons, statistically significant differences remained for iRES (adjusted P=0.001), Medigma (adjusted P=0.031), Straumann (adjusted P<0.001), and NTA (adjusted P=0.005). MAR was associated with lower artifact values for iRES and Straumann, whereas it was associated with higher values for Medigma and NTA. The adjusted comparisons were not statistically significant for Bilim, DTI, Medentika, Meisinger, Mode, Venus, or Neodent (Table 2).

Based on the paired brand-level mean values, the overall mean artifact value decreased from 41.08 in the non-MAR condition to 37.89 in the MAR condition. This corresponded to a mean reduction of 3.19 gray value units, or approximately 7.8%. The Hodges–Lehmann estimate of the paired difference was 3.19 gray value units (95% CI: −2.47 to 7.77), and the overall difference was not significant according to the Wilcoxon signed-rank test (P=0.206). MAR activation was associated with lower mean artifact values in eight of the 11 evaluated implant specimens and higher values in three. The greatest percentage reductions were observed for Straumann (27.9%) and iRES (26.2%), followed by Bilim (18.1%), Medentika (16.2%), and Mode (13.4%). In contrast, artifact values increased for Medigma (23.3%), NTA (21.0%), and Meisinger (2.2%) after MAR activation (Table 3).

Discussion

This in vitro experiment characterized CBCT gray value behavior around 11 commercially available dental implant brands and assessed the effect of MAR activation. The overall brand-level mean gray value decreased from 41.08 to 37.89 (a 7.8% reduction); however, this difference was not significant (P=0.206). Therefore, the null hypothesis could not be rejected. The magnitude and direction of the MAR-related changes differed between the evaluated implant specimens. Artifact values decreased in eight specimens and increased in three. After adjustment for multiple comparisons, significant reductions remained for iRES and Straumann, whereas Medigma and NTA showed significant increases. Because only one representative implant was evaluated for each brand, these results should be regarded as brand-related gray value trends rather than evidence of definitive statistical superiority or inferiority among implant systems. The non-significant overall Wilcoxon result should not be interpreted as indicating a uniform absence of a MAR effect across all evaluated specimens. Rather, it may reflect the bidirectional nature of the observed changes, whereby reductions in some specimens were counterbalanced by increases in others when the paired brand-level values were combined. Consequently, the overall mean provides only a limited summary of MAR performance in this heterogeneous dataset and should be interpreted alongside the direction and magnitude of

specimen-level changes. Nevertheless, because only one implant represented each brand, the implant-specific analyses remain exploratory and cannot establish generalized brand-level effects.

These findings are relevant to CBCT-based peri-implant assessment because implant-related artifacts may obscure the bone–implant interface and the peri-implant regions where cortical defects or marginal bone loss should be evaluated. Recent in vitro studies show that CBCT and MAR protocols should be assessed by diagnostic task rather than image appearance alone.[19,20]

In the non-MAR condition, Straumann, iRES, and Mode showed the highest descriptive gray value artifact measurements, whereas Medigma, DTI, and NTA showed the lowest values. This observation supports the view that implants with similar dimensions may still produce different CBCT artifact profiles under standardized acquisition conditions. Previous studies have shown that artifact formation around dental implants may be influenced by material composition, FOV, voxel size, exposure parameters, and the surrounding medium.[21–24] Although the present study compared implant brands rather than isolated materials, the observed variation may partly reflect differences in alloy composition, macrodesign, surface characteristics, and internal connection geometry.

Implant brand itself should not be considered an independent physical determinant of artifact formation. Rather, each brand represents a combination of implant-specific material and design characteristics that may influence x-ray attenuation and the resulting artifact pattern. Previous studies have demonstrated that implant material and composition can affect the magnitude and spatial distribution of CBCT artifacts, with titanium, titanium–zirconium, and zirconium dioxide implants producing different gray value alterations under comparable imaging conditions.[9,11,12] Differences in material density and effective atomic number may alter the extent of beam hardening, photon starvation, and scatter around the implant. In addition, variations in implant dimensions and the spatial distribution of highly attenuating material may modify the intensity and morphology of the resulting artifact. Because MAR algorithms identify and correct projection data affected by highly attenuating objects, differences in the intensity and spatial distribution of the original artifact may result in non-uniform responses to MAR activation. Previous evidence has also shown that MAR performance may vary by implant material, distance from the implant, and acquisition parameters.[14,25] Nevertheless, because implant composition and design characteristics were not independently analyzed and only one implant represented each brand, these mechanisms should be regarded as plausible explanations rather than definitive brand-specific causal conclusions.

A particular strength of the experimental design was independently scanning each implant within the same standardized phantom. This approach minimized adjacency-related artifact interactions and allowed each implant specimen to be evaluated separately under identical conditions. Martins et al.[16] showed that metal artifact expression increased when more metallic objects were positioned adjacent to the evaluated region, indicating that both the number and spatial arrangement of metallic objects may influence artifact magnitude.[16] Implant position, prosthetic components, and the scanned volume may also affect artifact expression.[26,27] These findings support the decision to avoid placing multiple implants within the same phantom, as the resulting gray value measurements could otherwise reflect the combined effects of the evaluated implant and adjacent metallic objects.

Using a standardized low-density wax phantom reduced variability caused by patient anatomy, movement, cortical thickness, trabecular architecture, and adjacent restorations. However, phantom selection itself can influence artifact expression. This represents a major limitation of the present experimental design because wax does not reproduce the differential radiodensities and atomic compositions of cortical bone, trabecular bone, and surrounding soft tissues. Beam hardening and scatter depend on the density and atomic number of the surrounding medium; therefore, the magnitude and spatial distribution of implant-related artifacts may differ between

the wax phantom and clinical peri-implant tissues. Studies using dry mandibles, bovine bone, dental arch phantoms, or dental-material phantoms show that artifact magnitude may change with the surrounding medium, geometry, and reconstruction environment.[21,23,28] Therefore, the wax phantom used in the present study should be considered a controlled experimental background rather than a direct simulation of clinical peri-implant bone conditions. Accordingly, the artifact profiles observed in this study should not be assumed to mirror those encountered in clinical peri-implant imaging. This limitation is important because peri-implantitis assessment in vivo involves cortical and trabecular bone, soft tissues, saliva, prosthetic restorations, and possible adjacent metallic objects.

MAR activation was associated with lower artifact values in eight of the 11 evaluated implant specimens and higher values in three, showing that the direction and magnitude of the response were not uniform. After Holm adjustment, statistically significant reductions remained for iRES and Straumann, whereas Medigma and NTA showed significant increases. This heterogeneous response is consistent with recent evidence indicating that MAR performance is task-, device-, protocol-, and material-dependent. Mancini et al.[25] reported that artifact behavior around titanium and zirconia implants varied according to distance from the implant, tube current, and MAR activation.[25] Capel et al.[29] showed that MAR level can influence assessment of dental implant positioning relative to the mandibular canal, with high MAR decreasing diagnostic accuracy compared with medium MAR and MAR-off conditions.[29] Studies evaluating MAR for detecting implant-related injuries to the inferior alveolar canal have also shown that the effect of MAR may vary by observer assessment and injury type.[20] These findings are clinically important because a quantitative decrease in artifact values does not automatically guarantee better diagnostic accuracy.

In the present study, Straumann and iRES showed the largest percentage reductions after MAR activation, whereas DTI and Venus showed only small numerical reductions. In contrast, MAR was associated with increased artifact values for Medigma, NTA, and Meisinger. After Holm adjustment, the reductions observed for Straumann and iRES, and the increases observed for Medigma and NTA remained statistically significant. This pattern suggests that MAR may interact differently with artifact profiles produced by different implant systems. Projection-domain MAR approaches may involve identifying metal-affected regions and replacing or correcting the corresponding projection data through interpolation or related reconstruction procedures. Although these approaches can reduce metal artifacts, interpolating affected projection data may also reduce adjacent structural information, leave residual artifacts, or introduce secondary artifacts.[30] Because the proprietary MAR procedure used by the CBCT system in the present study has not been publicly characterized in sufficient technical detail, its exact correction mechanism cannot be determined. Nevertheless, differences in the spatial distribution and geometric complexity of highly attenuating material might alter the extent and configuration of metal-affected projection data. Closely spaced threads, abrupt dimensional transitions, or dense internal connection regions could therefore create more complex correction requirements and contribute to incomplete or non-uniform correction. Such mechanisms might partly explain the increased gray value measurements observed for the Medigma and NTA specimens; however, this interpretation remains speculative. Implant geometry, internal connection characteristics, and alloy composition were not independently quantified, and the internal operation of the applied MAR algorithm was unavailable. Therefore, no causal relationship could be established between specific implant characteristics and the observed MAR responses. Further studies incorporating controlled material characterization, quantitative assessment of implant macrogeometry and internal connection design, and comparisons across different MAR algorithms are required to verify these hypotheses. Similar concerns have been raised in diagnostic studies in which MAR improved visual appearance in some cases but reduced confidence or diagnostic performance in specific tasks.[8,20,29]

The observed overall numerical reduction of 7.8% should be interpreted with caution because the corresponding brand-level comparison was not statistically significant. Moreover, MAR did not produce a consistently reductive effect across the evaluated specimens. Quantitatively, MAR produced a measurable change in peri-implant gray-value behavior under the tested protocol. Clinically, however, the relevance of this change depends on whether the reconstructed image improves visualization of peri-implant bone. Studies focused on peri-implant defects emphasize that MAR should be assessed using clinically relevant endpoints, such as detection of dehiscence, fenestration, marginal bone loss, or implant contact with anatomical structures.[19,20,29] Accordingly, these results indicate non-uniform MAR-related changes in brand-associated gray value profiles, but they do not establish improved diagnostic accuracy for peri-implantitis.

Artifact measurements were obtained at standardized coronal, middle, and apical axial levels, and corresponding ROI values were averaged to represent gray value alterations along the longitudinal extent of the implant body. This multi-level sampling approach reduced dependence on a single axial plane while maintaining standardized ROI positioning across all implant specimens and reconstruction conditions. The purpose was to compare relative peri-implant gray value profiles under identical experimental conditions rather than to quantify the total three-dimensional artifact volume. Nevertheless, this approach does not constitute full volumetric analysis and may not capture the complete spatial propagation of metal artifacts. Another important issue is that CBCT gray values are not standardized in the same way as Hounsfield units in medical CT. For this reason, gray value measurements were used as relative indicators of artifact expression rather than absolute density values. Recent CBCT artifact studies continue to use gray value-based measurements, histogram-based analysis, or profile-plot approaches for quantitative artifact assessment.[21,23,24,28] This supports the methodological approach used in the present study, provided that the values are interpreted within the same CBCT unit and scanning protocol. The present design, in which all implants were scanned using the same device, FOV, voxel size, kVp, mA, exposure time, and reconstruction protocol, was therefore essential for maintaining internal consistency.

The present findings should be interpreted as quantitative observations of MAR-related changes in gray value artifact profiles under standardized experimental conditions. A reduction in measured gray value alteration does not necessarily indicate improved visualization of the bone–implant interface or greater accuracy in detecting marginal bone loss, dehiscence, fenestration, or peri-implantitis. Because the study did not include simulated bone defects, clinical tissues, or observer-based diagnostic assessment, no conclusions can be drawn regarding the effect of MAR on diagnostic performance or treatment planning. Further studies using clinically relevant defect models and diagnostic accuracy outcomes are required to determine whether the observed quantitative changes provide a clinically meaningful benefit.

Several limitations should be considered when interpreting the findings. First, the experiment was conducted in vitro using a standardized wax phantom, which does not fully reproduce the complexity of clinical peri-implant imaging. Second, the study did not include simulated peri-implantitis defects, marginal bone loss, fenestrations, dehiscences, or prosthetic suprastructures; therefore, it evaluated quantitative gray value alterations rather than diagnostic accuracy. Third, only one CBCT device and one acquisition protocol were used, and the results may differ with other devices or scanning conditions. Fourth, although implant dimensions were comparable, the exact alloy composition, surface chemistry, thread profile, and internal connection morphology were not independently analyzed. Fifth, only one representative implant was evaluated for each brand. Although repeated acquisitions and multiple ROI measurements allowed standardized characterization of each tested specimen, they did not represent independent implant samples. Therefore, intra-brand variability related to manufacturing tolerances, implant models, dimensions, thread configurations, or alloy

composition could not be assessed. Consequently, the findings should be interpreted as descriptive profiles of the evaluated specimens. Future studies including multiple independent implants from each brand would help assess the reproducibility of these patterns within individual implant systems. Sixth, although artifact measurements were obtained at standardized coronal, middle, and apical axial levels, a full three-dimensional volumetric assessment of artifact distribution was not performed.

Future studies should include multiple implants from each brand, different implant diameters and lengths, controlled material characterization, and clinically relevant peri-implant defect models. Further research should also compare MAR-on and MAR-off reconstructions across different CBCT units, FOVs, voxel sizes, tube voltages, and tube currents. Diagnostic accuracy studies using observer-based evaluation would be particularly valuable to determine whether the quantitative changes observed in artifact values translate into improved detection of peri-implantitis-related bone defects.

Conclusion

The implant specimens evaluated in this controlled in vitro study showed variable CBCT gray value profiles and different quantitative responses to MAR activation. Although the overall mean artifact measurement was numerically lower with MAR, the overall brand-level difference was not significant. After adjustment for multiple comparisons, significant reductions were observed for the iRES and Straumann specimens, whereas significant increases were observed for Medigma and NTA, demonstrating that MAR did not produce a uniformly reductive effect. Because only one representative implant was assessed for each brand, the findings cannot establish intra-brand reproducibility or characterize the overall radiographic behavior of the corresponding implant systems. When CBCT is used for peri-implant bone assessment, both implant-related gray value behavior and the limitations of MAR reconstruction should be considered. Because the analysis was performed in a wax phantom and was based on quantitative gray value measurements, the results should be interpreted as experimental artifact profile data rather than direct evidence of improved diagnostic accuracy for peri-implantitis.

Acknowledgments

Not applicable.

Authors' Contributions

Conceptualization: Onur Sahar
Data curation: Onur Sahar and Sema Kaya
Formal analysis: Onur Sahar and Sema Kaya
Funding acquisition: Onur Sahar and Sema Kaya
Investigation: Onur Sahar and Sema Kaya
Methodology: Onur Sahar and Sema Kaya
Project administration: Onur Sahar and Sema Kaya
Resources: Onur Sahar and Sema Kaya
Software: Sema Kaya
Supervision: Sema Kaya
Validation: Onur Sahar and Sema Kaya
Visualization: Sema Kaya
Writing—original draft: Onur Sahar and Sema Kaya
Writing—review and editing: Onur Sahar and Sema Kaya

Competing Interests

The authors declare no competing interests related to this study. No implant manufacturer had any role in the study design, CBCT acquisition, image analysis, statistical evaluation, interpretation of the results, or preparation of the manuscript.

Data Availability

The datasets generated and/or analyzed during the current study are available from the corresponding author upon reasonable request.

Ethics Approval

Not applicable. This study was designed as an in vitro experimental material study using commercially available dental implant materials. It did not involve human participants, human-derived tissues, animals, patient records, or identifiable patient data.

Funding

This research was self-funded and received no specific grant from funding agencies in the public, commercial, or not-for-profit sectors.

References

1. Buser D, Sennerby L, De Bruyn H. Modern implant dentistry based on osseointegration: 50 years of progress, current trends and open questions. Periodontol 2000. 2017;73(1):7-21. doi:10.1111/prd.12185.
2. Berglundh T, Armitage G, Araujo MG, Avila-Ortiz G, Blanco J, Camargo PM, et al. Peri-implant diseases and conditions: Consensus report of workgroup 4 of the 2017 World Workshop on the Classification of Periodontal and Peri-Implant Diseases and Conditions. J Clin Periodontol. 2018;45 Suppl 20:S286-S291. doi:10.1111/jcpe.12957.
3. Schwarz F, Derks J, Monje A, Wang HL. Peri-implantitis. J Clin Periodontol. 2018;45 Suppl 20: S246-S266. doi:10.1111/jcpe.12954.
4. Scarfe WC, Farman AG. What is cone-beam CT and how does it work? Dent Clin North Am. 2008;52(4):707-30. doi:10.1016/j.cden.2008.05.005.
5. Bornstein MM, Scarfe WC, Vaughn VM, Jacobs R. Cone beam computed tomography in implant dentistry: a systematic review focusing on guidelines, indications, and radiation dose risks. Int J Oral Maxillofac Implants 2014;29 Suppl:55-77. doi:10.11607/jomi.2014suppl.g1.4.
6. Kamburoğlu K, Murat S, Kılıç C, Yüksel S, Avsever H, Farman A, et al. Accuracy of CBCT images in the assessment of buccal marginal alveolar peri-implant defects: effect of field of view. Dentomaxillofac Radiol. 2014;43(4):20130332. doi:10.1259/dmfr.20130332.
7. de-Azevedo-Vaz SL, Vasconcelos Kde F, Neves FS, Melo SL, Campos PS, Haiter-Neto F. Detection of peri-implant fenestration and dehiscence with the use of two scan modes and the smallest voxel sizes of a cone-beam computed tomography device. Oral Surg Oral Med Oral Pathol Oral Radiol. 2013;115(1):121-7. doi:10.1016/j.oooo.2012.10.003.
8. Schulze R, Heil U, Gross D, Bruellmann DD, Dranischnikow E, Schwanecke U, et al. Artefacts in CBCT: a review. Dentomaxillofac Radiol. 2011;40(5):265-73. doi:10.1259/dmfr/30642039.
9. Pauwels R, Stamatakis H, Bosmans H, Bogaerts R, Jacobs R, Horner K, et al. Quantification of metal artifacts on cone beam computed tomography images. Clin Oral Implants Res. 2013; 24 Suppl A100:94-9. doi:10.1111/j.1600-0501.2011.02382.x.
10. Benic GI, Sancho-Puchades M, Jung RE, Deyhle H, Hämmerle CHF. In vitro assessment of artifacts induced by titanium dental implants in cone beam computed tomography. Clin Oral Implants Res. 2013;24(4):378-83. doi:10.1111/clr.12048.

11. Sancho-Puchades M, Hämmerle CH, Benic GI. In vitro assessment of artifacts induced by titanium, titanium-zirconium and zirconium dioxide implants in cone-beam computed tomography. Clin Oral Implants Res. 2015;26(10):1222-8. doi:10.1111/clr.12438.
12. Terrabuio BR, Carvalho CG, Peralta-Mamani M, Santos PSDS, Rubira-Bullen IRF, Rubira CMF. Cone-beam computed tomography artifacts in the presence of dental implants and associated factors: an integrative review. Imaging Sci Dent. 2021;51(2):93-106. doi:10.5624/isd.20200320.
13. Machado AH, Fardim KAC, de Souza CF, Sotto-Maior BS, Assis NMSP, Devito KL. Effect of anatomical region on the formation of metal artefacts produced by dental implants in cone beam computed tomographic images. Dentomaxillofac Radiol. 2018;47(3):20170281. doi:10.1259/dmfr.20170281.
14. Parsa A, Ibrahim N, Hassan B, Syriopoulos K, van der Stelt P. Assessment of metal artefact reduction around dental titanium implants in cone beam CT. Dentomaxillofac Radiol. 2014;43(7):20140019. doi:10.1259/dmfr.20140019.
15. de-Azevedo-Vaz SL, Peyneau PD, Ramirez-Sotelo LR, Vasconcelos Kde F, Campos PS, Haiter-Neto F. Efficacy of a cone beam computed tomography metal artifact reduction algorithm for the detection of peri-implant fenestrations and dehiscences. Oral Surg Oral Med Oral Pathol Oral Radiol. 2016;121(5):550-6. doi:10.1016/j.oooo.2016.01.013.
16. Martins LAC, Queiroz PM, Nejaim Y, Vasconcelos KF, Groppo FC, Haiter-Neto F. Evaluation of metal artefacts for two CBCT devices with a new dental arch phantom. Dentomaxillofac Radiol. 2020;49(5):20190385. doi:10.1259/dmfr.20190385.
17. Bosshardt DD, Chappuis V, Buser D. Osseointegration of titanium, titanium alloy and zirconia dental implants: current knowledge and open questions. Periodontol 2000. 2017;73(1):22-40. doi:10.1111/prd.12179.
18. Cahyaningtyas NA, Miranda A, Metta P, Bawono CA. Dental implant macrodesign features in the past 10 years: A systematic review. J Indian Soc Periodontol. 2023;27(2):131-9. doi:10.4103/jisp.jisp_676_21.
19. Nomier AS, Gaweesh YSE, Taalab MR, El Sadat SA. Efficacy of low-dose cone beam computed tomography and metal artifact reduction tool for assessment of peri-implant bone defects: an in vitro study. BMC Oral Health. 2022;22(1):615. doi:10.1186/s12903-022-02663-8.
20. Soltani P, Devlin H, Etemadi Sh M, Rengo C, Spagnuolo G, Baghaei K. Do metal artifact reduction algorithms influence the detection of implant-related injuries to the inferior alveolar canal in CBCT images? BMC Oral Health. 2024;24(1):268. doi:10.1186/s12903-024-04043-w.
21. Vahdani N, Moudi E, Ghobadi F, Mohammadi E, Bijani A, Haghanifar S. Evaluation of the metal artifact caused by dental implants in cone beam computed tomography images. Maedica (Bucur). 2020;15(2):224-9. doi:10.26574/maedica.2020.15.2.224.
22. Kuzu TE, Kiş HC. Effect of different cone beam computed tomography settings on artifact production in titanium and zirconia dental implants: an in vitro study. Dent Med Probl. 2024;61(2):233-9. doi:10.17219/dmp/157233.
23. Hinchy NV, Anderson NK, Mahdian M. Metal artifact reduction using common dental materials. Dentomaxillofac Radiol. 2022;51(2):20210302. doi:10.1259/dmfr.20210302.
24. Shokri A, Vafaee F, Haghighat L, Shahabi S, Farhadian M, Jamalpour MR. Comparison of the amount of artifacts induced by zirconium and titanium implants in cone-beam computed tomography images. BMC Med Imaging. 2022;22(1):156. https://doi.org/10.1186/s12880-022-00884-5.
25. Mancini AXM, Santos MUC, Gaêta-Araujo H, Tirapelli C, Pauwels R, Oliveira-Santos C. Artefacts at different distances from titanium and zirconia implants in cone-beam computed tomography: effect of tube current and metal artefact reduction. Clin Oral Investig. 2021; 25(8):5087-5094. doi:10.1007/s00784-021-03821-y.

26. Gurjar BS, Sharma V, Paliwal J, Kalla R, Meena KK, Tahir M. The role of implants and implant prostheses on the accuracy and artifacts of cone-beam computed tomography: an in-vitro study. Sci Rep. 2024;14(1):704. doi:10.1038/s41598-024-51293-3.
27. Fardim KAC, Machado AH, Assis NMSP, Sotto-Maior BS, Mauad LQ, Devito KL. Artifacts caused by titanium implants in CBCT images of the mandible: an experimental study. Gen Dent. 2022;70(1):72-7.
28. Andrade-Bortoletto MFS, Fontenele RC, Farias-Gomes A, Freitas DQ. Mapping artifacts generated in a tooth adjacent to titanium and zirconia implants located in the endomass and exomass in cone beam computed tomography: an ex vivo study. Oral Surg Oral Med Oral Pathol Oral Radiol. 2024;137(1):73-82. doi:10.1016/j.oooo.2023.08.002.
29. Capel CP, da Motta RJG, Pauwels R, Gaêta-Araujo H, Oliveira-Santos C, Tirapelli C. Effect of metal artefact reduction level on the assessment of dental implant positioning by cone-beam computed tomography. Dentomaxillofac Radiol. 2024;53(4):233-9. doi:10.1093/dmfr/twae008.
30. Tang H, Lin YB, Jiang SD, Li Y, Li T, Bao XD. A new dental CBCT metal artifact reduction method based on a dual-domain processing framework. Phys Med Biol. 2023;68(17):175016. doi:10.1088/1361-6560/acec29.

Table 1. Descriptive statistics and 95% confidence intervals for gray value artifact measurements obtained without and with MAR

Implant	Non-MAR mean ± SD (95% CI)	With MAR mean ± SD (95% CI)	Mean difference (non-MAR − MAR), 95% CI
Bilim	42.84±8.74 (39.14–46.53)	35.07±10.14 (30.79–39.35)	7.77 (2.25–13.29)
DTI	34.14±5.65 (31.76–36.53)	32.92±8.77 (29.22–36.63)	1.22 (−2.82–5.26)
IRES	45.65±8.46 (42.08–49.22)	33.71±8.12 (30.28–37.14)	11.94 (6.73–17.16)
Medentika	41.89±7.46 (38.75–45.04)	35.09±8.95 (31.31–38.87)	6.81 (2.03–11.59)
Medigma	34.03±8.37 (30.50–37.56)	41.96±11.58 (37.07–46.85)	−7.93 (−13.02 to −2.84)
Meisinger	40.47±11.01 (35.82–45.12)	41.37±14.24 (35.36–47.38)	−0.90 (−7.02–5.23)
Mode	45.27±13.23 (39.68–50.85)	39.20±9.00 (35.40–43.00)	6.07 (0.14–12.00)
Straumann	47.18±15.14 (40.78–53.57)	34.03±8.37 (30.50–37.56)	13.15 (8.12–18.17)
Venus	42.72±7.65 (39.49–45.95)	40.83±13.18 (35.26–46.39)	1.90 (−4.82–8.61)
Neodent	40.32±8.17 (36.87–43.76)	37.41±12.81 (32.00–42.82)	2.91 (−4.15–9.96)
NTA	37.42±9.44 (33.44–41.41)	45.27±13.23 (39.68–50.85)	−7.84 (−12.22 to −3.46)

Values are presented as mean ± standard deviation and 95% confidence interval. Mean differences were calculated as non-MAR minus MAR; therefore, positive values indicate lower artifact measurements following MAR application. CI, confidence interval; MAR, metal artifact reduction.

Table 2. Exploratory ROI-level paired comparisons of gray value measurements obtained without and with MAR

Implant	N	Non-MAR (Mean ± SD)	With MAR (Mean ± SD)	Unadjusted P-value	Holm-adjusted P-value
Bilim	24	42.84±8.74	35.07±10.14	0.011	0.063
DTI	24	34.14±5.65	32.92±8.77	0.491	1.000
iRES	24	45.65±8.46	33.71±8.12	<0.001	0.001
Medentika	24	41.89±7.46	35.09±8.95	0.009	0.061
Medigma	24	34.03±8.37	41.96±11.58	0.004	0.031
Meisinger	24	40.47±11.01	41.37±14.24	0.877	1.000
Mode	24	45.27±13.23	39.20±9.00	0.060	0.302
Straumann	24	47.18±15.14	34.03±8.37	<0.001	<0.001
Venus	24	42.72±7.65	40.83±13.18	0.491	1.000
Neodent	24	40.32±8.17	37.41±12.81	0.406	1.000
NTA	24	37.4 ±9.44	45.27±13.23	<0.001	0.005

Data are presented as mean ± standard deviation. Unadjusted P-values were calculated using exploratory ROI-level Wilcoxon signed-rank tests comparing paired measurements obtained from corresponding non-MAR and MAR reconstructions. Holm-adjusted P-values account for the 11 implant-specific comparisons and were used to determine statistical significance. Statistical significance was set at an adjusted $P<0.05$. N represents the number of composite ROI-level measurements per implant under each reconstruction condition. MAR, metal artifact reduction; ROI, region of interest; SD, standard deviation.

Table 3. Summary of MAR effect for each implant brand: mean differences and percentage changes

Implant	Non-MAR (Mean ± SD)	With MAR (Mean ± SD)	Difference	Change (%)	Direction
Straumann	47.18±15.14	34.03±8.37	13.15	27.9%	↓
iRES	45.65±8.46	33.71±8.12	11.94	26.2%	↓
Bilim	42.84±8.74	35.07±10.14	7.77	18.1%	↓
Medentika	41.89±7.46	35.09±8.95	6.81	16.2%	↓
Mode	45.27±13.23	39.20±9.00	6.07	13.4%	↓
Neodent	40.32±8.17	37.41±12.81	2.91	7.2%	↓
Venus	42.72±7.65	40.83±13.18	1.90	4.4%	↓
DTI	34.14±5.65	32.92±8.77	1.22	3.6%	↓
Meisinger	40.47±11.01	41.37±14.24	−0.90	−2.2%	↑
NTA	37.42±9.44	45.27±13.23	−7.84	−21.0%	↑
Medigma	34.03±8.37	41.96±11.58	−7.93	−23.3%	↑

Difference was calculated as non-MAR minus MAR. Positive values indicate a reduction, whereas negative values indicate an increase following MAR activation. MAR, metal artifact reduction; SD, standard deviation.

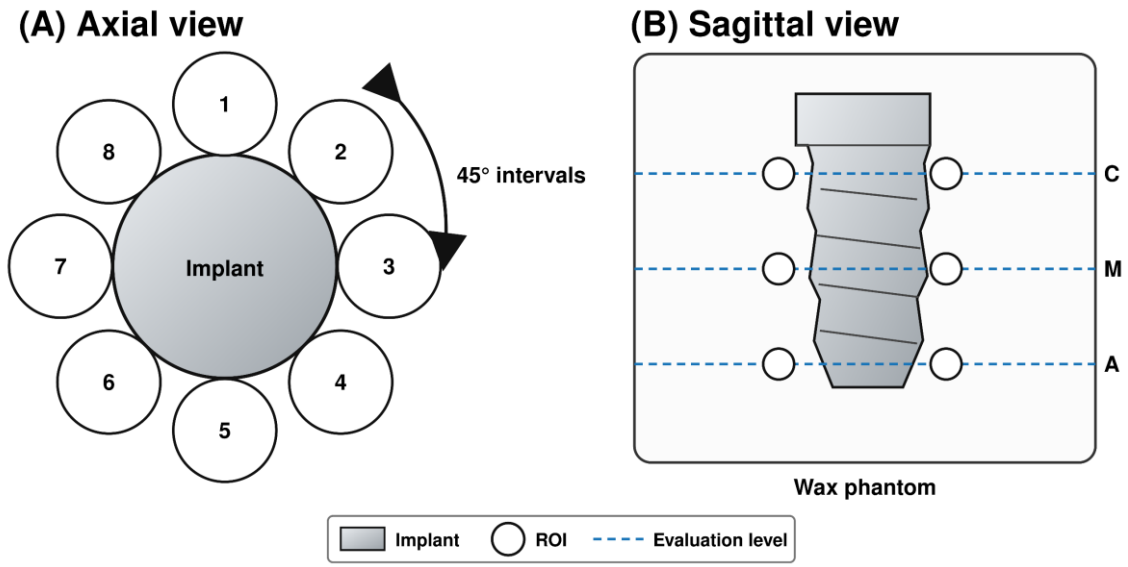

Figure 1. Schematic representation of the standardized peri-implant gray value measurement procedure. The sagittal view shows the coronal (C), middle (M), and apical (A) levels selected along the implant body, while the corresponding axial view demonstrates the circumferential placement of eight standardized circular regions of interest (ROIs) at 45° intervals. Each ROI had a diameter of 3.0 mm (10 pixels), an area of 7.20 mm², and was positioned immediately adjacent to the implant surface without overlapping the implant body. Measurements obtained from corresponding ROI positions at the coronal, middle, and apical levels were averaged to generate eight composite ROI values for each scan. C, coronal; M, middle; A, apical; ROI, region of interest.